Hydrodynamic Models of Viscous Coupling between Motile Myosin and Endoplasm in Characean Algae

EUGENE A. NOTHNAGEL and W. W. WEBB
School of Applied and Engineering Physics, Cornell University, Ithaca, New York 14853. Dr. Nothnagel's present address is the Department of Chemistry, University of Colorado, Boulder, Colorado 80309.

ABSTRACT Cytoplasmic streaming in characean algae is thought to be driven by interaction between stationary subcortical actin bundles and motile endoplasmic myosin. Implicit in this mechanism is a requirement for some form of coupling to transfer motive force from the moving myosin to the endoplasm. Three models of viscous coupling between myosin and endoplasm are presented here, and the hydrodynamic feasibility of each model is analyzed. The results show that individual myosinlike molecules moving along the actin bundles at reasonable velocities cannot exert enough viscous pull on the endoplasm to account for the observed streaming. Attachment of myosin to small spherical organelles improves viscous coupling to the endoplasm, but results for this model show that streaming can be generated only if the myosin-spheres move along the actin bundles in a virtual solid line at about twice the streaming velocity. In the third model, myosin is incorporated into a fibrous or membranous network or gel extending into the endoplasm. This network is pulled forward as the attached myosin slides along the actin bundles. Using network dimensions estimated from published micrographs of characean endoplasm, the results show that this system can easily generate the observed cytoplasmic streaming.

Actin-myosin interactions are thought to be responsible for the generation of many types of biological motility, including muscle contraction, amoeboid movement, cytoplasmic streaming, phagocytosis, cell division, and axonal transport (1). Although it is now generally understood how the interaction between actin and myosin leads ultimately to the motion (contraction) of muscle tissue, in most nonmuscle systems the details of motion generation are not yet understood (1). In particular, detailed mechanisms are lacking for the hypothesized actin-myosin-driven flow of intracellular fluid in amoeboid movement, cytoplasmic streaming, and axonal transport. Implicit in these proposed actin-myosin systems is the assumption that the sliding of myosin molecules past actin bundles is somehow coupled to the intracellular fluid to produce a bulk flow.

The purpose of this paper is to examine, from a hydrodynamic viewpoint, the feasibility of various supramolecular structures that might function to provide coupling between actin-myosin sliding and bulk fluid flow. The hydrodynamics presented will be modeled for the geometry of cytoplasmic streaming in characean algae. Various microscopic, ultrastructural, and biochemical observations (2–5) have provided evi-

dence that this streaming is driven by actin-myosin. Although other mechanisms have been proposed (6), most available evidence (3) suggests that characean streaming is driven by interaction between motile endoplasmic myosin and stationary subcortical actin bundles (Fig. 1). The highly organized pattern of streaming in characean internodal cells makes this a convenient system for hydrodynamic modeling. Some of the results obtained for this system may then find applications in other, less organized, nonmuscle systems.

A number of theoretical studies considering the fluid mechanics of characean streaming have been published (6–12). Most of these previous studies (6, 9–11) considered only the bulk flow of endoplasm and cell sap. Two studies (8, 12) did include treatment of the flow in the boundary layer near the endoplasm-ectoplasm interface, but did not consider mechanisms by which the sliding motion of myosin molecules along actin bundles might be coupled to the endoplasm.

The present work begins with a short summary of established empirical characteristics of cytoplasmic streaming in characean algae. Several models for the viscous coupling of myosin motion to the endoplasm are then presented and evaluated in terms of these characteristics.
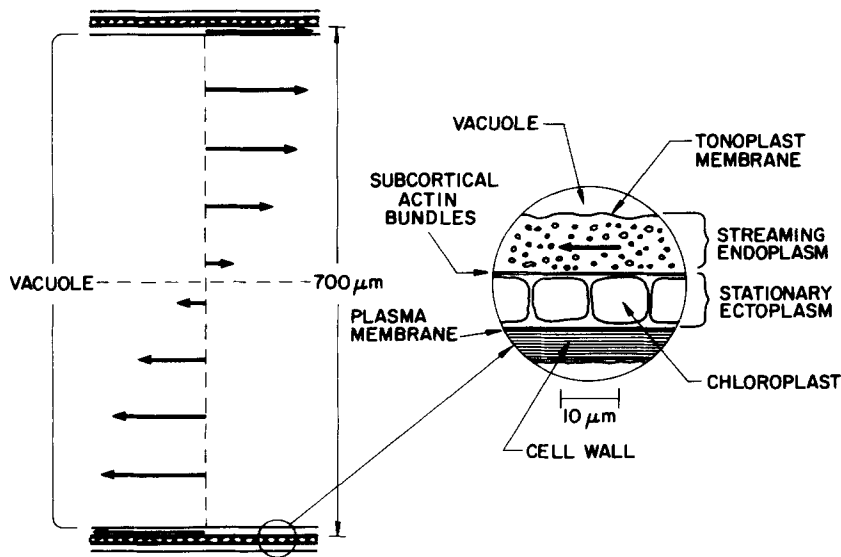
FIGURE 1 Longitudinal section of a segment of a characean internodal cell. The heavy arrows indicate streaming velocity. The magnified field shows structure near the cell wall.

EMPIRICAL CHARACTERISTICS OF CYTOPLASMIC STREAMING IN CHARACEAN INTERNODAL CELLS

Cell Size

Mature internodal cells of characean algae reach lengths of up to 10 cm and diameters of up to 1 mm. The stationary ectoplasm and chloroplasts are positioned just inside the plasma membrane (Fig. 1). Adjoining the inside face of the ectoplasm is the 10-μm-thick layer of flowing endoplasm. The inside boundary of the endoplasm is the tonoplast membrane that surrounds the large vacuole in the center of the cell. A typical internodal cell has a length of 4 cm and a cylindrical endoplasm-ectoplasm interface of diameter 700 μm.

Velocity Characteristics

STREAMING VELOCITY: Casual microscopic examination of characean internodal cells reveals endoplasmic streaming at rates up to 100 μm/s. A rate of 80 μm/s is typical.

VELOCITY PROFILE: The velocity gradient in the endoplasm is very small everywhere except in the immediate vicinity of the endoplasm-ectoplasm interface (9, 13, 14). The velocity of the endoplasm is 0 at this interface but increases rapidly away from the interface, reaching essentially full streaming velocity within a distance corresponding approximately to the depth of field of a high-power microscope objective (0.5 μm or less). The cell sap in the vacuole flows with the endoplasm at the tonoplast and then slows smoothly to 0 velocity at the center of the vacuole where the opposing streams meet (Fig. 1).

This velocity profile was interpreted (14) as evidence that cytoplasmic streaming is not a Poiseuille-like flow driven by some pressure difference over the length of the cell. Rather, motive force generation occurs at or near the endoplasm-ectoplasm interface (14) and is, like viscous dissipation, a localized process.

VELOCITY HISTOGRAM: Cytoplasmic streaming has been studied by laser-light scattering to obtain velocity histograms indicating the relative amount of endoplasm flowing at each velocity in the cell (15–20). Laser-light scattering is a more sensitive technique for velocity analysis than is simple microscope observation, because light scattering can detect non-visual events such as fluctuations in refractive index due to concentration fluctuations (15). Velocity histograms obtained

with either the Doppler (15, 16, 18, 19) or the correlation (17, 20) technique are in close agreement and show that most of the endoplasm moves with velocities falling in a narrow range around the most probable velocity. The most probable velocity corresponds very closely to the velocity of the bulk endoplasm as measured by light microscopy. Various velocity histograms (16, 18, 19) all show rapid decline at velocities greater than the most probable velocity, and there is no evidence to suggest that any endoplasmic component moves faster than about two times the most probable velocity.

Motive Force

The magnitude of the force driving streaming has been estimated by using either centrifugation (21) or vacuolar perfusion (7, 22) to apply to a reverse balancing force. Expressed per unit area of the endoplasm-ectoplasm interface, the motive force measured by either method is 1–4 dyn/cm^2.

Fluid Viscosities

CELL SAP VISCOSITY: The viscosity of the vacuolar cell sap falls in the range of 1–2.5 centipoise (cP) (7, 13, 23).

ENDOPLASMIC VISCOSITY: Although several measurements of endoplasmic viscosity have been reported (6, 7, 9, 11, 12, 23, 24), there remains considerable uncertainty regarding the rheological properties of the endoplasm. By forcing isolated *Nitella* endoplasm through an agar capillary, Kamiya and Kuroda (23, 24) found that the endoplasm exhibits the non-Newtonian characteristic of decreased apparent viscosity at increased shear rate. The apparent viscosity is 50–250 cP at shear rates 30–100 times smaller than the shear rate near the endoplasm-ectoplasm interface in streaming cells. Viscosity measurements at higher shear rates were not reported (23, 24). Other non-Newtonian studies suggest that the viscosity coefficient of streaming endoplasm *in situ* may be an order of magnitude smaller than that of isolated endoplasm (7).

Some experiments (6, 9) suggest that endoplasm in intact cells behaves as a simple Newtonian fluid. Endoplasmic viscosity in *Nitella* cells is 6 cP when determined by analysis of the Brownian motion of 0.3–0.4 μm endoplasmic particles (6).

Subcortical Actin Bundles

About four actin bundles (25) of diameter 0.1–0.2 μm (6, 26, 27) are attached to each chloroplast file at the endoplasm-

ectoplasm interface (Fig. 1). These bundles run parallel to the direction of streaming (27) and are spaced ~0.7 μm apart on a given chloroplast file. The spacing between bundles on different, adjacent files is somewhat larger (25), however, so the spacing comes to about 2 μm when averaged over several chloroplast files.

THREE MODELS OF VISCOUS COUPLING BETWEEN MOTILE MYOSIN AND THE ENDOPLASM

Each of the three hydrodynamic models of streaming considered in this paper assumes that the characean endoplasm contains myosinlike molecules that hydrolyze ATP and slide along the subcortical actin bundles in a process analogous to muscle contraction. The models differ in the manner by which viscous coupling is utilized to transfer this sliding force to the endoplasm and thereby enable cytoplasmic streaming.

Several simplifying assumptions will be made in analyzing the hydrodynamics of the three models. Among these simplifications will be the treatment of the endoplasm and cell sap as simple Newtonian fluids, and the use of planar geometry rather than the actual cylindrical geometry of the algal cell. Although some precision is lost through this approach (see Appendix D), the essential hydrodynamics are retained in a readily tractable form with accuracy sufficient for evaluation of the three models.

Several general hydrodynamic characteristics of streaming are revealed by estimating the Reynolds number (28, 29) for flow in a characean internodal cell. The Reynolds number R is the ratio of inertial forces to viscous forces (28, 30) and is given by

$$R = \frac{l v \rho}{\eta}, \quad (1)$$

where l is a characteristic dimension (cm), v is the fluid velocity (cm/s), ρ is the fluid density (g/cm^3), and η is the fluid viscosity [g/cm·s) = poise]. For the streaming endoplasm, $l \simeq 10$ μm, $v \simeq 80$ μm/s, $\rho \simeq 1$ g/cm^3, and $\eta \simeq 6$ cP (6), so that $R \simeq 10^{-4}$. Likewise, for flow in the vacuole R is no more than $R \simeq 0.05$. These very small Reynolds numbers show that the effect of inertia is negligible and guarantee that cytoplasmic streaming is turbulence-free (28).

Model A: Myosinlike Molecules Dispersed in the Endoplasm

This model assumes that the myosinlike molecules are individually dispersed in the endoplasm and are coupled to the fluid and endoplasmic organelles by viscous forces only. Maximum motive force is exerted on the endoplasm when the number of moving myosin molecules is large enough to effectively cover the subcortical actin bundles. The myosin-covered actin bundles are then essentially equivalent to circular cylinders moving longitudinally along the endoplasm-ectoplasm interface. Viscous drag between the moving cylinders and the surrounding fluid serves to transmit the motive force to the endoplasm.

The motive force generated by such a system can be estimated from a Stokes-like formula for the drag between a cylinder and surrounding fluid in relative motion. To utilize such a formula, however, the endoplasmic velocity near the endoplasm-ectoplasm interface must be known. Since the velocity profile in this region is not well characterized empirically

(Empirical Characteristics: Velocity Profile), it is necessary to estimate this velocity theoretically. Such an estimate follows from an assumption regarding the spatial distribution of motive force generation in the cell.

Available information concerning the velocity profile of streaming (see Empirical Characteristics: Velocity Profile) suggests that motive force generation is localized along the endoplasm-ectoplasm interface. Following the approach of Donaldson (7) then, the motive force F is taken as a constant per unit volume in a thin layer along this interface. This assumption is posed formally as shown in Fig. 2a, where the endoplasm-ectoplasm interface is the $y = 0$ plane, and the direction of streaming is along the $+z$ axis. The tonoplast membrane is at $y = \delta$ and is assumed to transmit shear forces as a vanishingly thin layer of viscous fluid (9). The center of the vacuole is at $y = \gamma$. Region I, $0 \leq y \leq \epsilon$, represents the region of motive force generation and has a thickness comparable to the diameter of the subcortical actin bundles (0.1–0.2 μm; see Empirical Characteristics: Subcortical Actin Bundles). In Region I the motive force is $F = F_z$, where F_z is a constant vector pointing in the $+z$ direction and has units of force per unit volume. In Region II, $\epsilon \leq y \leq \delta$, and Region III, $\delta \leq y \leq \gamma$, $F = 0$. The endoplasm in each region is assigned a viscosity η_i and density ρ_i; $i = 1, 2, 3$, respectively.

From this spatial distribution of motive force, the velocity profile throughout the cell can be calculated (see Appendix A). A typical result is shown in Fig. 2b and is in good agreement with available experimental data (Empirical Characteristics: Velocity Profile). Expressions for several important physical quantities can also be calculated (Appendix A) for this model. F_{za}, the applied motive force per unit area of endoplasm-ectoplasm interface, is simply

$$F_{za} = F_z\epsilon. \quad (2)$$

By comparison, F_{zw}, the drag on the endoplasm-ectoplasm interface wall, is

$$F_{zw} = F_z\epsilon\kappa. \quad (3)$$

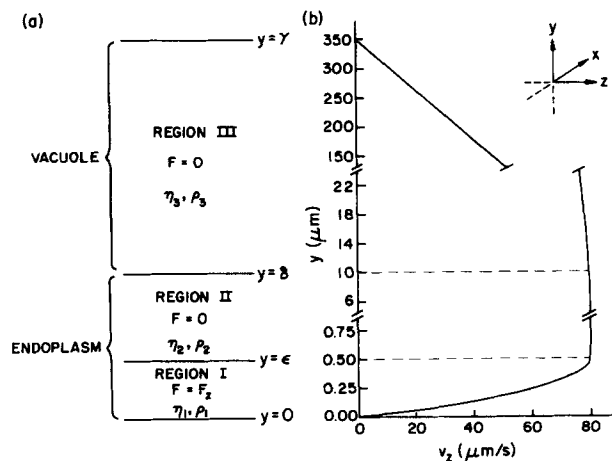Both F_{za} and F_{zw} have units of force per unit area. The

FIGURE 2 Segment of a characean internodal cell in simplified geometry for Models A and B. (a) Division of the cell into three regions, each characterized by a motive force per unit volume F, fluid viscosity η_i, and fluid density ρ_i. (b) Velocity profile calculated from Eqs. A-10–A-12. Parameters used in the calculation were taken from parameter set 1B of Table II. Note the scale changes along the y-axis. The x-axis points into the plane of the paper.

dimensionless parameter κ (defined by Eq. A-14 in Appendix A) takes the value 1 in the absence of the vacuole ($\eta_3 = 0$). The extent to which the value of κ falls below 1 is a measure of the influence of the vacuole on streaming. Finally, the maximum velocity in the cell, v_{zm}, occurs in Region I at $y = \kappa\epsilon$ and is

$$v_{zm} = \frac{F_z \epsilon^2 \kappa^2}{2\eta_1}. \tag{4}$$

Using the velocity profile calculated for Region I (Fig. 2b), the maximum motive force that could be generated by myosin molecules moving along the subcortical actin bundles is now estimated. The myosin molecules are assumed to cover the actin bundles to form moving cylinders of diameter ϵ, the thickness of Region I. The center-to-center spacing between the parallel cylinders is s, and they move longitudinally through Region I with a velocity expressed hv_{zm} where v_{zm} is the maximum streaming velocity (Eq. 4), and h is a dimensionless speed factor. The total motive force F_{za} that this array of moving cylinders exerts on the endoplasm per unit area of endoplasm-ectoplasm interface is estimated in Appendix A as

$$F_{za} = \frac{2\pi\eta_1 v_{zm}}{s[\ln(2s/\epsilon) - 1.32]}\left[h - \frac{(\kappa - 3/8)}{\kappa^2}\right]. \tag{5}$$

Eq. 2 gives an alternate expression for F_{za}. Equating these two expressions for F_{za}, using Eq. 4, and solving for the speed factor h gives the result:

$$h = \frac{s}{\pi\epsilon\kappa^2}[\ln(2s/\epsilon) - 1.32] + \frac{(\kappa - 3/8)}{\kappa^2}. \tag{6}$$

All of the parameters on the right side of Eq. 6 can be estimated (see Empirical Characteristics). Hence, Eq. 6 represents a key test of the feasibility of this model. Myosin must slide along the actin bundles at a speed hv_{zm} if the endoplasm is to move at speed v_{zm}. This model of streaming is hydrodynamically feasible only if the velocity hv_{zm} is reasonable.

Numerical results for this model are presented in Table I, where seven different sets of input parameters are considered. In the absence of the vacuole ($\eta_3 = 0$), both the dimensionless parameter κ (Eq. A-14) and the velocity ratio $v_z(\delta)/v_{zm}$ [$v_z(\delta)$ is the velocity at $y = \delta$ and v_{zm} is from Eq. 4] take the value 1. For all sets of input parameters in Table I, $\kappa \simeq 1$ and $v_z(\delta)/v_{zm} \simeq 1$ with high precision, indicating a negligible effect of the vacuole on streaming.

The most important results in Table I, however, are the values for the speed factor h (Eq. 6) and the applied force per unit area F_{za} (Eq. 5). The speed factor h is ~6 for reasonable

actin bundle diameter ϵ and spacing s (parameter sets 1A–4A). This value for h does not change over a wide range of values for the viscosities η_1 and η_2 (parameter sets 1A–4A). Somewhat smaller values for h result if larger effective bundle diameters or closer bundle spacings are allowed (parameter sets 5A–7A).

Unlike the results for h, the calculated values for the motive force F_{za} increase rapidly with increasing η_1 (Table I). The viscosity η_2, however, has a negligible effect on F_{za} (parameter sets 2A–3A). Lower motive force is required with larger effective bundle diameters (parameter sets 5A and 6A, cf. 1A and 2A).

Model B: Myosinlike Molecules Attached to Small Spherical Organelles

The viscous drag that a moving myosin molecule could exert on the endoplasm would be increased if the myosin were covalently attached to an object larger than itself. It has been suggested (31, 32) that characean myosin may be associated with small endoplasmic organelles. The hydrodynamics of this system can be investigated by assuming that the moving myosin molecules are attached to small spheres. As these spheres are pulled along the subcortical actin bundles, viscous Stokes drag (28, 29) between the spheres and the surrounding fluid serves to transmit the motive force to the endoplasm.

To estimate the motive force that could be delivered to the endoplasm by such a system of moving spheres, it is again necessary to know the velocity profile near the endoplasm-ectoplasm interface. The theoretical profile (Fig. 2b) calculated for Model A can also be used for this system of moving spheres. Likewise, Eqs. 2–4 are again valid.

With this theoretical velocity profile, the motive force generated by the system of moving spheres can be estimated. The center-to-center spacing between actin bundles is again s, and the diameter of the moving spheres is ϵ, the thickness of Region I (Fig. 2a). Let q be the center-to-center spacing between adjacent spheres on the same actin bundle, and let the velocity of the spheres be hv_{zm} where v_{zm} is from Eq. 4, and h is again a dimensionless speed factor. The total motive force F_{za} that this array of moving spheres exerts on the endoplasm per unit area of endoplasm-ectoplasm interface is then (Appendix B)

$$F_{za} = \frac{3\pi\eta_1\epsilon v_{zm}}{sq}\left[h - \frac{(\kappa - 1/3)}{\kappa^2}\right]. \tag{7}$$

Eq. 2 again gives an alternate expression for F_{za}. Equating these two expressions for F_{za} and using Eq. 4 gives an equation in q and h. Solving this equation for q gives

TABLE I

Numerical Evaluation of Model A—Dispersed Myosin

Parameter set	Input parameters					Calculated parameters			
	η_1	η_2	η_3	ϵ	s	κ	$v_z(\delta)/v_{zm}$	h	F_{za}
	cP	cP	cP	μm	μm				dyn/cm^2
1A	1	6	1	0.2	2	0.9997	0.995	5.96	8.0
2A	6	6	1	0.2	2	0.99995	0.995	5.96	48
3A	6	250	1	0.2	2	0.99995	0.9999	5.96	48
4A	250	250	1	0.2	2	0.999999	0.9999	5.96	2,000
5A	1	6	1	0.4	2	0.9994	0.995	2.19	4.0
6A	6	6	1	0.5	2	0.9999	0.995	1.59	19
7A	1	6	1	0.1	0.7	0.9999	0.995	3.57	16

The following additional input parameters were held constant for all calculations: $\delta = 10\ \mu m$, $\gamma = 350\ \mu m$ (see Figure 2 a), and $v_{zm} = 80\ \mu m/s$ (streaming velocity). ϵ is the effective diameter of the subcortical actin bundles, and s is the average spacing between the bundles. The speed factor h appears in hv_{zm}, the velocity of myosin along the actin bundles. The motive force F_{za} was calculated from Eq. 5. See text for other calculated parameters.

$$q = \frac{3\pi\epsilon^2\kappa^2}{2s}\left[h - \frac{(\kappa - 1/3)}{\kappa^2}\right], \tag{8}$$

whereas solving for h gives

$$h = \frac{2sq}{3\pi\epsilon^2\kappa^2} + \frac{(\kappa - 1/3)}{\kappa^2}. \tag{9}$$

With the exception of q and h, all of the parameters in Eqs. 8 and 9 can be estimated (see Empirical Characteristics). Hence Eqs. 8 and 9 represent a test of the feasibility of this model. According to this model, streaming is generated by spheres of diameter ϵ moving along the actin bundles. The center-to-center spacing between adjacent spheres on a bundle must be q, and the velocity of the spheres must be hv_{zm} if the endoplasm is to move at velocity v_{zm}. This model of streaming is hydro-dynamically feasible only if suitable q and h can be found to satisfy Eqs. 8 and 9. Workable solutions require a sphere spacing greater than the sphere diameter, $q > \epsilon$, and also a reasonable sphere velocity hv_{zm}.

Numerical results for this model are presented in Table II, where 10 different sets of input parameters are considered. As with Model A, the parameters κ and $v_z(\delta)/v_{zm}$ are always very nearly 1 and indicate a negligible effect of the vacuole on streaming.

The key results in Table II are the values of the speed factor h (Eq. 9), the sphere spacing q (Eq. 8), and the applied force per unit area F_{za} (Eq. 7). For a given sphere diameter ϵ, the minimum workable value for h is obtained when $q = \epsilon$ so that the spheres touch each other in a solid line along the actin bundles. For $\epsilon = 0.5$ μm sphere diameter, this minimum value for the speed factor is $h = 1.52$ (parameter sets 1B–4B). In this limit of a solid line of spheres, Model B should give results similar to Model A if the diameters of the spheres and cylinders are equal. Direct comparison of parameter sets 6A (Table I) and 2B (Table II) is possible and shows that Models A and B do yield very similar values for h (1.59 and 1.52, respectively).

Results for the parameter pair h and q do not change over a wide range of values for the viscosities η_1 and η_2 (parameter sets 1B–4B). Although the motive force F_{za} is similarly independent of η_2, its value increases rapidly with increasing η_1 (parameter sets 1B–4B).

Parameter sets 5B–8B show that sphere spacing q increases rapidly with increasing speed factor h. Hence, fewer spheres are required when they move more rapidly. Fewer or slower spheres are adequate if their diameters are increased (parameter sets 9B and 10B).

Model C: Myosinlike Molecules Attached to an Endoplasmic Network

Various ultrastructural studies have indicated the existence of a fibrous or membranous network in the endoplasm of characean cells (6, 25, 26, 32–34). The fluid mechanical implications of this network are considered in this model. It is assumed that myosinlike molecules are incorporated into, or are attached to, a three-dimensional network or gel existing in the endoplasm. As the myosin molecules move along the subcortical actin bundles, the attached network is pulled forward as well. Viscous drag between the network and surrounding fluid acts to transfer the motive force to the endoplasm.

For ease of calculation, the network is taken to be a cubic lattice of intersecting right circular cylinders. Such a network may be visualized as being somewhat similar to a wire test tube rack. At every point of intersection in the network there are three cylinders, one parallel to the x-axis, another parallel to the y-axis, and a third parallel to the z-axis. Let the radius of all the cylinders be a, and the center-to-center spacing between adjacent parallel cylinders be b, where $b \gg a$.

The algal cell is again divided into regions with the endoplasm occupying $0 \leq y \leq \delta$ (Fig. 3a). The network is assumed to exist throughout the endoplasm except within the thin Region I, $0 \leq y \leq \epsilon$, adjoining the endoplasm-ectoplasm interface ($y = 0$). Region I represents the space between the subcortical actin bundles where the network is not likely to enter, and hence its thickness corresponds to the actin bundle diameter. Region II, $\epsilon \leq y \leq \delta$, contains the network. Region III, $\delta \leq y \leq \gamma$, represents the vacuole and is bounded by the tonoplast ($y = \delta$) and the center of the vacuole ($y = \gamma$). Each region is assigned a fluid viscosity η_i and density ρ_i; $i = 1, 2, 3$, respectively.

Let v_n be the velocity at which myosin pulls the network along the actin bundles. In Regions I and III the motive force per unit volume applied to the fluid is $\mathbf{F} = 0$. In Region II the motive force $\mathbf{F}$ is directed along the z-axis and has magnitude equal to the drag between the network and the fluid. The local drag force depends on the difference between the network velocity v_n and the local fluid velocity v_z. Since the fluid

TABLE II

Numerical Evaluation of Model B—Myosin on Spheres

Parameter set	Input parameters					Calculated parameters				
	η_1	η_2	η_3	ϵ	s	κ	$v_z(\delta)/v_{zm}$	h	q	F_{za}
	cP	cP	cP	μm	μm				μm	dyn/cm^2
1B	1	6	1	0.5	2	0.9993	0.995	1.52	0.5	3.2
2B	6	6	1	0.5	2	0.9999	0.995	1.52	0.5	19
3B	6	250	1	0.5	2	0.9999	0.9999	1.52	0.5	19
4B	250	250	1	0.5	2	0.999997	0.9999	1.52	0.5	800
5B	1	6	1	0.5	2	0.9993	0.995	1.00	0.196	3.2
6B	1	6	1	0.5	2	0.9993	0.995	2.00	0.784	3.2
7B	1	6	1	0.5	2	0.9993	0.995	3.00	1.37	3.2
8B	1	6	1	0.5	2	0.9993	0.995	4.00	1.96	3.2
9B	1	6	1	0.9	2	0.9987	0.995	1.14	0.9	1.8
10B	1	6	1	0.9	2	0.9987	0.995	2.00	2.54	1.8

The following additional input parameters were held constant for all calculations: $\delta = 10$ μm, $\gamma = 350$ μm (see Figure 2 a), and $v_{zm} = 80$ μm/s (streaming velocity). ϵ is the diameter of the spheres, and s is the average spacing between subcortical actin bundles. The speed factor h appears in hv_{zm}, the velocity of spheres along the actin bundles. q is the center-to-center spacing between spheres. Workable solutions require $q \geq \epsilon$. The motive force F_{za} was calculated from Eq. 7. See text for other calculated parameters.
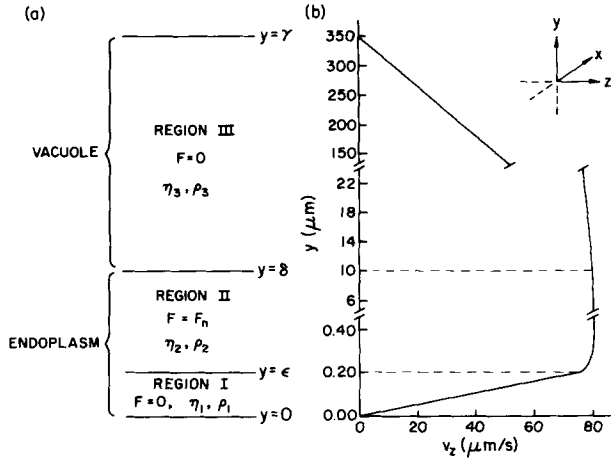
FIGURE 3 Segment of a characean internodal cell in simplified geometry for Model C. (a) Division of the cell into three regions, each characterized by a motive force per unit volume F, fluid viscosity η_i, and fluid density ρ_i. (b) Velocity profile calculated from Eqs. 13–16. Parameters used in the calculation were taken from parameter set 2C of Table III. Note the scale changes along the y-axis. The x-axis points into the plane of the paper.

velocity varies with y in *Region II*, the motive force also varies with y.

The solutions for both the velocity and the motive force are outlined in Appendix C. The solutions, Eqs. C-8–C-16, are generally complicated combinations of exponential functions. Three parameters appearing in these solutions are:

$$k = \frac{\sqrt{2\pi f}}{b},\tag{10}$$

$$\alpha = \frac{\eta_1}{\eta_2 k \epsilon},\tag{11}$$

$$\beta = \frac{\eta_3}{\eta_2 k(\gamma - \delta)}.\tag{12}$$

The parameter k has the dimension of inverse length, whereas α and β are dimensionless. Eq. C-4 in Appendix C defines f, a dimensionless parameter depending on b/a, the ratio of network dimensions.

Considerable simplification of Eqs. C-8–C-16 of Appendix C is possible when the values of the parameters k, δ, and ϵ are such that $k(\delta - \epsilon) \gg 1$. Under these conditions the fluid velocity v_z can be approximated as follows.

In *Region I*, valid for $k(\delta-\epsilon) \gg 1$ and $0 \le y \le \epsilon$:

$$v_z = \frac{v_n y}{\epsilon} \frac{(1 + \beta)}{(1 + \alpha + \beta + \alpha\beta)}.\tag{13}$$

In *Region II*, valid for $k(\delta - \epsilon) \gg 1$ and $\epsilon \le y \le \delta/2$:

$$v_z = v_n \left[1 - \frac{\alpha(1 + \beta)}{(1 + \alpha + \beta + \alpha\beta)} e^{-k(y - \epsilon)} \right].\tag{14}$$

In *Region II*, valid for $k(\delta - \epsilon) \gg 1$ and $2\delta/3 < y \le \delta$:

$$v_z = v_n \left[1 - \frac{\beta(1 + \alpha)}{(1 + \alpha + \beta + \alpha\beta)} e^{-k(\delta - y)} \right].\tag{15}$$

In *Region III*, valid for $k(\delta - \epsilon) \gg 1$ and $\delta \le y \le \gamma$:

$$v_z = v_n \frac{(\gamma - y)}{(\gamma - \delta)} \frac{(1 + \alpha)}{(1 + \alpha + \beta + \alpha\beta)}.\tag{16}$$

The motive force F_{za} applied per unit area of the endoplasm-ectoplasm interface takes the following simplified form when $k(\delta - \epsilon) \gg 1$:

$$F_{za} = \frac{v_n \eta_1}{\epsilon} \frac{[1 + (\beta/\alpha) + 2\beta]}{(1 + \alpha + \beta + \alpha\beta)}.\tag{17}$$

Likewise, when $k(\delta - \epsilon) \gg 1$ the drag F_{zw} exerted by the moving endoplasm on the endoplasm-ectoplasm interface wall is given by

$$F_{zw} = \frac{v_n \eta_1}{\epsilon} \frac{(1 + \beta)}{(1 + \alpha + \beta + \alpha\beta)}.\tag{18}$$

Both F_{za} and F_{zw} have dimensions of force per unit area.

The maximum velocity in the cell occurs at $y = y_m$, where

$$y_m = \frac{1}{2} \left\{ \delta + \epsilon + \frac{1}{k} \ln \left[\frac{\alpha + \alpha\beta}{\beta + \alpha\beta} \right] \right\}.\tag{19}$$

Eq. 19 is valid provided that the mathematical conditions $k(\delta - y_m) \gg 1$ and $k(y_m - \epsilon) \gg 1$ are met.

Eqs. 13–19 together represent a key test of the feasibility of this model. The network dimensions a (cylinder radius) and b (spacing between cylinders) can be estimated from published electron micrographs of characean endoplasm (25, 26, 32–34). The remaining input parameters can be estimated from previous measurements (see Empirical Characteristics). Results predicted, then, for the velocity profile (Eqs. 13–16) and motive force (Eq. 17) must be consistent with the Empirical Characteristics if this model of streaming is to be hydrodynamically feasible.

Numerical results for this model are presents in Table III, where 11 different sets of input parameters are considered. The network dimensions a and b of parameter set 1C were estimated from Figs. 11 and 12 of reference 34. The fibrous networks shown in Figs. 1 and 2 of reference 25 were used to estimate the a and b of parameter set 2C. The network dimensions for sets 3C and 4C were estimated from the membranous network shown in Fig. 3 of reference 33.

Some general results from Table III are noted. The smallest value obtained for $k(\delta - \epsilon)$ is $k(\delta - \epsilon) = 59$. Thus the mathematical requirement $k(\delta - \epsilon) \gg 1$ is well satisfied for all parameter sets 1C–11C, and Eqs. 13–19 are excellent approximations for the exact solutions, Eqs. C8–C16 of Appendix C. Fig. 3 b shows a typical velocity profile calculated from Eqs. 13–16. This velocity profile, showing a large velocity gradient in *Region I* and almost constant velocity in *Region II*, is in good agreement with available experimental data (Empirical Characteristics: Velocity Profile).

The relative velocity at $y = \delta$, $v_z (\delta)/v_n$, is essentially 1 for all parameter sets listed in Table III. The ratio of wall drag to applied force, F_{zw}/F_{za}, can be calculated from Eqs. 17 and 18 with the result $1 > (F_{zw}/F_{za}) \ge 0.999$ for all parameter sets of Table III. These results for $v_z (\delta)/v_n$ and F_{zw}/F_{za} together show that flow in the vacuole has a negligible effect on streaming in *Regions I* and *II*.

Key results for the velocity profile and the applied force per unit area, F_{za}, are included in Table III. Properties of the velocity profile are indicated by y_m, the coordinate corresponding to the maximum streaming velocity in the cell, and by $y_{0.9}$, the coordinate in *Region I* or *II* corresponding to the point at which the streaming velocity reaches 0.9 v_n (90% of the network velocity) in its increase away from the wall. Parameter sets 1C–4C show that y_m and $y_{0.9}$ increase modestly as the network

Numerical Evaluation of Model C—Myosin on Endoplasmic Network

Parameter set	Input parameters						Calculated parameters				
	η_1	η_2	η_3	a	b	ϵ	$k(\delta - \epsilon)$	$v_z(\delta)/v_n$	y_m	$y_{0.9}$	F_{za}
	cP	cP	cP	μm	μm	μm			μm	μm	dyn/cm^2
1C	1	6	1	0.01	0.1	0.2	507	0.99999	5.17	0.183	3.9
2C	1	6	1	0.04	0.3	0.2	195	0.99998	5.29	0.188	3.8
3C	1	6	1	0.06	0.7	0.2	68	0.99993	5.63	0.210	3.6
4C	1	6	1	0.1	0.9	0.2	59	0.99992	5.71	0.232	3.5
5C	1	1	1	0.04	0.3	0.2	195	0.99985	5.28	0.235	3.2
6C	1	250	1	0.04	0.3	0.2	195	0.999999	5.29	0.180	4.0
7C	6	6	1	0.04	0.3	0.2	195	0.99998	5.33	0.235	19
8C	6	250	1	0.04	0.3	0.2	195	0.999999	5.33	0.181	24
9C	250	250	1	0.04	0.3	0.2	195	0.999999	5.42	0.235	799
10C	1	1	1	0.1	0.9	0.2	59	0.99951	5.67	0.451	2.2
11C	1	1	1	0.04	0.3	0.1	197	0.99985	5.24	0.161	5.3

The following additional input parameters were held constant for all calculations: $\delta = 10\,\mu m$, $\gamma = 350\,\mu m$ (see Fig. 3 a), and $v_n = 80\,\mu m/s$ (network velocity). a is the radius of the network cylinders, b is the spacing between the cylinders, and ϵ is the thickness of the Region I boundary layer (see Figure 3 a). y_m is the coordinate of the maximum velocity in the cell and was calculated from Eq. 19. $y_{0.9}$ is the coordinate in Region I or II at which the streaming velocity reaches $0.9\,v_n$ and was calculated from Eq. 13 or 14. The motive force F_{za} was calculated from Eq. 17. See text for other parameters.

dimensions a and b increase through a wide range of values. The applied force F_{za} decreases slightly over the same ranges of a and b.

Parameter sets 2C and 5C–9C of Table III show that large changes in the viscosities η_1 and η_2 produce only small changes in the velocity profile indicators y_m and $y_{0.9}$. As with Models A and B, the applied force F_{za} increases rapidly with increasing η_1. Unlike Models A and B, however, this model also shows small but significant increases of F_{za} with increasing η_2.

Parameters sets 5C and 10C, with $\eta_1 = \eta_2 = \eta_3 = 1$, present the case of a low viscosity "ground plasm" surrounding the network. This small value for η_2 leads to a smaller velocity gradient at the wall, as indicated by larger values of $y_{0.9}$ and smaller values of F_{za}. Parameter set 11C presents the case of a thinner network-free boundary layer in Region I. A smaller thickness ϵ results in a larger velocity gradient as indicated by a smaller $y_{0.9}$ and a larger F_{za}.

DISCUSSION

Model A: Dispersed Myosin Cannot Drive Cytoplasmic Streaming

Very high myosin velocities are required in a system where the myosin molecules are simply dispersed in the endoplasm without permanent linkage to endoplasmic organelles. For reasonable actin bundle diameter and spacing (Empirical Characteristics: Subcortical Actin Bundles), myosin must slide along the actin bundles at a velocity about six times faster than the streaming velocity in order to overcome boundary drag and drive the bulk flow (Table I, parameter sets 1A–4A).

This high velocity requirement appears to be inconsistent with the measured velocity histogram which shows no evidence for any motions faster than about two times the most probable streaming velocity (Empirical Characteristics: Velocity Histogram). In addition, it has been noted (35) that the velocity of streaming, 80 $\mu m/s$, is already several times greater than the maximum velocity of actin-myosin sliding in the fastest striated muscle, 30 $\mu m/s$. Hence, Model A appears unfeasible also because the required speed of characean actin-myosin would be not merely 2.7 but rather 16 times faster than muscle actin-myosin.

The data in Table I show that this high velocity requirement is relaxed somewhat if larger cylinder diameters ϵ are allowed.

The required cylinder diameters are, however, several times larger than the known diameter of the actin bundles (Empirical Characteristics: Subcortical Actin Bundles).

These results for Model A are based on the assumption that the actin bundles are completely covered by moving myosin so that maximum motive force is attained. Hence the speed factors in Table I represent minimum estimates, and even these speed factors are prohibitively large. The inadequacy of this system arises from the fact that actin bundles cover only a small fraction of the surface area of the endoplasm-ectoplasm interface. Retarding drag exerted on the endoplasm by the relatively large areas between the bundles can be overcome only by very high velocities on the actin bundles. Yano et al. (36, 37) have reported streaming of heavy meromyosin solutions in narrow channels formed by walls containing immobilized actin filaments. Streaming in this artificial system presumably occurs only when a large fraction of the wall area is covered by attached actin.

Model B: Myosin-spheres Are Only Marginally Capable of Driving Streaming

A more effective viscous coupling between myosin and the endoplasm occurs in a system where myosin is attached to the surface of small organelles (31, 32) or spheres. The observed pattern of streaming could be generated by 0.5 μm diameter spheres moving along the actin bundles at about twice the endoplasmic velocity, but then the number of spheres required would form essentially a solid line along the bundles (Table II, parameter sets 1B–4B, 6B).

If the velocity of the spheres exceeds twice the endoplasmic velocity, then the required number of spheres is less (Table II). As noted with Model A, however, these higher velocities are inconsistent with both the measured velocity histogram of streaming and the known speed of muscle actin-myosin contraction. Fewer spheres will also suffice if their diameters are enlarged to 0.9 μm (Table II, parameter sets 9B, 10B). Although ultrastructural studies (32) have shown that organelles as large as 0.9 μm are present in perfused characean cells, casual light microscopic observation of intact cells suggests that most endoplasmic organelles are 0.5 μm or smaller and that the number of larger organelles is too limited to produce the required density along the bundles.

Although the myosin-spheres of Model B represent a hydrodynamic improvement over the dispersed myosin of Model A, generation of streaming by this system of spheres is still only marginal at best. In its favored version, this system requires movement of a solid line of 0.5 μm spheres along each actin bundle. Since characean endoplasm does contain large numbers of as yet uncharacterized 0.5 μm organelles, this model of streaming cannot be completely excluded. If the real generator of streaming does resemble this model, then the marginal adequacy of the hydrodynamic coupling of myosin-spheres to the endoplasm may act as an inherent governor on streaming.

Model C: Myosin on an Endoplasmic Network Can Easily Drive Streaming

Observed cytoplasmic streaming can be easily generated if myosinlike molecules are attached to, or incorporated into, a fibrous or membranous network extending into the endoplasm. Although available ultrastructural studies (25, 26, 32–34) provide only tentative morphological details on the endoplasmic network, such details are adequate for this calculation because the hydrodynamics of the system are not strongly dependent on the network dimensions. Dimensions estimated from any of several published micrographs showing endoplasmic networks (25, 33, 34) all give results (Table III, parameter sets 1C–4C) consistent with the Empirical Characteristics.

For most parameter sets listed in Table III, ~90% of the velocity increase occurs within *Region I*, the 0.1–0.2 μm thick transition layer between the wall and the network (Fig. 3 *a*). This very rapid velocity increase away from the wall evidences the thorough coupling between the network and the endoplasmic fluid. This thorough coupling is responsible for a major feature of Model C—the endoplasm streams at the velocity of the endoplasmic network. There is no requirement for motions faster than streaming itself. This result is in good agreement with the measured velocity histogram (Empirical Characteristics: Velocity Histogram) and minimizes the requirement for a high speed actin-myosin interaction.

Although Model C assumes the existence of the network throughout *Region II*, the calculated velocity profile (Fig. 3 *b*) shows that this requirement can be relaxed. The network exerts no viscous pull on the endoplasm in those areas where the network and endoplasm move at the same speed. Hence the network is indispensable only within the first two or three lattice spacings along the $y = \epsilon$ boundary of *Region II*. The network may then resemble a thin sheet more than a three-dimensional structure. Thin membranous networks of appropriate dimensions are shown in several published electron micrographs (26, 33).

Likewise the rigid, cubic lattice structure of the network represents only a convenience for calculation rather than a strict necessity. Tangled, random, or elastic networks may also suffice. Streaming could likewise be driven by a dynamic network that occasionally breaks and reforms. Small motile organelles observed in both intact and perfused cells (31–33) may be fragments that have separated from the network either spontaneously or as a result of shear forces experienced during perfusion. These separated organelles may work together with the network in intact cells to generate streaming by a combined Model B and Model C mechanism.

Models A–C share the result that nearly all of the applied motive force acts to overcome the drag force at the endoplasm-ectoplasm interface wall, i.e., $F_{za} \simeq F_{zw}$. This important result is an inherent property of streaming and is not limited to

Models A–C. Several previous theoretical studies of cytoplasmic streaming (6, 8, 10) have overlooked the importance of the drag force at the wall.

The property $F_{za} \simeq F_{zw}$ implies that the main conclusions of this study hold valid over a wide range of endoplasmic viscosities. In particular, the speed factors h calculated for Models A and B (Tables I and II) are essentially independent of the endoplasmic viscosities η_1 and η_2. This feature arises because both the motive force F_{za} and the wall drag F_{zw} are viscous forces that depend almost linearly on η_1 and negligibly on η_2. In the balance of these forces $(F_{za} \simeq F_{zw})$ the strong dependence on η_1 cancels out. Likewise indicators of the Model C velocity profile $(y_m$ and $y_{0.9}$ in Table III) change only slightly with large changes in η_1 and η_2. Lingering uncertainties regarding the rheological properties of the endoplasm (Empirical Characteristics: Endoplasmic Viscosity), therefore, do not alter the feasibilities of Models A–C.

A parameter that does depend strongly on endoplasmic viscosity is the motive force F_{za}. For all Models A–C, F_{za} increases almost linearly with increasing boundary layer viscosity η_1 (Tables I–III), and results comparable to the measured 1–4 dyn/cm² forces (Empirical Characteristics: Motive Force) are calculated only when η_1 is ~1 cP. Since viscosity is defined as the ratio of shear stress to shear rate (28, 30), this low boundary layer viscosity follows inevitably from the measured motive force (≈ 2 dyn/cm²; Empirical Characteristics: Motive Force) and the large velocity gradient near the endoplasm-ectoplasm interface (≈ 160 s⁻¹; Empirical Characteristics: Velocity Profile).

The hydrodynamic considerations presented here show that myosinlike molecules sliding along subcortical actin bundles cannot alone exert enough viscous pull to produce streaming of the endoplasm in characean cells. Attachment of the myosin to small spherical organelles improves viscous coupling to the endoplasm but leads to a system that is only marginally capable of producing the observed streaming. Cytoplasmic streaming can be easily generated when myosin is attached to a fibrous or membranous network extending into the endoplasm. Although these calculations modeled streaming for the geometry of characean cells, similar considerations may be relevant for other forms of motility, including axonal transport and amoeboid movement. The suggestion that myosin is attached to endoplasmic organelles may have important implications for biochemical and ultrastructural characterization of myosin and associated proteins in these systems.

APPENDIX A: VELOCITY PROFILE ESTIMATION AND MOTIVE FORCE GENERATED BY AN ARRAY OF MOVING CYLINDERS

The velocity profile of streaming is calculated for the distribution of motive force shown in Fig. 2 *a*. Donaldson (7) has solved a related problem for a non-Newtonian fluid. Here the fluid is taken to be Newtonian and incompressible, so the general equation of motion giving the fluid velocity **v** is the Navier-Stokes equation (28):

$$\frac{\partial \mathbf{v}}{\partial t} + (\mathbf{v} \cdot \nabla)\mathbf{v} = -\frac{1}{\rho}\nabla p + \frac{\eta}{\rho}\nabla^2\mathbf{v} + \frac{\mathbf{F}}{\rho} + \mathbf{g}, \qquad (A\text{-}1)$$

where t is time, p is pressure, **g** is gravity, ρ is the fluid density, η is the fluid viscosity, and **F** is the impressed force per unit volume. For cytoplasmic streaming the force of gravity is negligible (9). The steady state, time-independent solution is sought for very small Reynolds number flow. Under these conditions Eq. A-1 takes the form (29):

$$-\nabla p + \eta\nabla^2\mathbf{v} + \mathbf{F} = 0. \qquad (A\text{-}2)$$

The remaining equation of motion is the continuity equation for an incompressible fluid (28):

$$\nabla \cdot \mathbf{v} = 0. \tag{A-3}$$

There are no applied gradients in the pressure p. This condition, together with the applied force per unit volume and simplified geometry of Fig. 2a, requires that $\mathbf{v} = v_z$, i.e., fluid flows only in the z direction in all *Regions I–III*. Furthermore, v_z is independent of x and z and depends only on y. Eq. A-3 is then satisfied identically, and Eq. A-2 takes the following forms in the three regions.

In *Region I:*

$$\eta_1 \frac{d^2 v_z}{dy^2} + F_z = 0. \tag{A-4}$$

In *Regions II and III:*

$$\frac{d^2 v_z}{dy^2} = 0. \tag{A-5}$$

It also follows that the presure within each region must be a constant.

The boundary conditions on the fluid velocity (28) are:

$$v_z = 0 \text{ at } y = 0 \text{ and } y = \gamma \tag{A-6}$$

and

$$v_z \text{ continuous at } y = \epsilon \text{ and } y = \delta. \tag{A-7}$$

At the interfaces between the regions, the forces that the adjoining fluids exert on each other must be equal and opposite (28) so that:

$$\eta_1 \left(\frac{dv_z}{dy} \right)_I = \eta_2 \left(\frac{dv_z}{dy} \right)_{II} \quad \text{at } y = \epsilon \tag{A-8}$$

and

$$\eta_2 \left(\frac{dv_z}{dy} \right)_{II} = \eta_3 \left(\frac{dv_z}{dy} \right)_{III} \quad \text{at } y = \delta, \tag{A-9}$$

where the derivatives are calculated from the v_z expressions for the indicated regions. The pressure must also be continuous at the interfaces and hence is a constant throughout the cell.

Eqs. A-4 and A-5 with boundary conditions A-6–A-9 can be solved by straightforward techniques (38) to give:

in *Region I* ($0 \leq y \leq \epsilon$),

$$v_z = \frac{F_z}{2\eta_1} (2\epsilon\kappa y - y^2); \tag{A-10}$$

in *Region II* ($\epsilon \leq y \leq \delta$),

$$v_z = \frac{F_z \epsilon^2}{2\eta_1 \lambda} [\eta_3(\delta - y) + \eta_2(\gamma - \delta)]; \tag{A-11}$$

in *Region III* ($\delta \leq y \leq \gamma$),

$$v_z = \frac{F_z \epsilon^2 \eta_2}{2\eta_1 \lambda} (\gamma - y). \tag{A-12}$$

The parameter λ is given by the expression

$$\lambda = \left\{ \eta_2(\gamma - \delta) + \eta_3 \left[\delta + \epsilon \left(\frac{\eta_2}{\eta_1} - 1 \right) \right] \right\}, \tag{A-13}$$

and κ is a dimensionless parameter given by

$$\kappa = \left(1 - \frac{\eta_2 \eta_3 \epsilon}{2\eta_1 \lambda} \right). \tag{A-14}$$

Eq. A-10 can be differentiated to find the maximum velocity in the cell, v_{zm}:

$$v_{zm} = \frac{F_z \epsilon^2 \kappa^2}{2\eta_1} \text{ at } y = \kappa\epsilon. \tag{A-15}$$

The force per unit volume F_z is a constant throughout the ϵ-thick *Region I.* F_{za}, the applied motive force per unit area of endoplasm-ectoplasm interface, is then

$$F_{za} = F_z \epsilon. \tag{A-16}$$

The drag F_{zw} on the endoplasm-ectoplasm interface wall is calculated from the velocity gradient at the wall:

$$F_{zw} = F_z \epsilon \kappa. \tag{A-17}$$

The motive force exerted on the endoplasm by cylinders of myosin moving longitudinally in *Region I* can be estimated from a Stokes-like formula for the drag between a cylinder and surrounding fluid in relative motion. Consider right circular cylinders of radius a arranged in a square array such that all cylinders are mutually parallel, with s being the center-to-center spacing between nearest neighbors. For low Reynolds number fluid flow between cylinders in a dilute ($s \gg a$) array, the drag force per unit length on each cylinder is approximately

$$F_a = \frac{2\pi\eta U}{\ln(s/a) - 1.32}, \tag{A-18}$$

where the direction of fluid flow is parallel to the axes of the cylinders (29). In this equation, $\pi = 3.1416$, η is the viscosity of the fluid, and U is the superficial (average) velocity of fluid flow through the array.

In applying Eq. A-18 to the streaming problem, the average velocity U is replaced by the difference between hv_{zm}, the velocity of myosin moving along the actin bundles, and $\overline{v_{zc}}$, the effective average velocity of the endoplasm in *Region I* as seen by the cylinder. If the cylinder of radius a is centered at $y = \epsilon/2$ in *Region I*, then averaging the Eq. A-10 velocity over the surface area of the cylinder gives the result (39):

$$\overline{v_{zc}} = \frac{F_z}{2\eta_1} [\epsilon^2(\kappa - 1/4) - a^2/2]. \tag{A-19}$$

Taking the radius of the cylinder as $a = \epsilon/2$ and using Eqs. A-15, A-18, and A-19, the force exerted on the endoplasm per unit length of actin bundle becomes:

$$F_a = \frac{2\pi\eta_1 v_{zm}}{\ln(2s/\epsilon) - 1.32} \left[h - \frac{(\kappa - 3/8)}{\kappa^2} \right]. \tag{A-20}$$

Since the spacing between actin bundles is s, the total force exerted on the endoplasm per unit area of endoplasm-ectoplasm interface is F_a/s, or

$$F_{za} = \frac{2\pi\eta_1 v_{zm}}{s[\ln(2s/\epsilon) - 1.32]} \left[h - \frac{(\kappa - 3/8)}{\kappa^2} \right]. \tag{A-21}$$

APPENDIX B: MOTIVE FORCE GENERATED BY AN ARRAY OF MOVING SPHERES

The motive force exerted on the endoplasm by myosin-drawn spheres can be estimated from the Stokes formula for the drag force F_s on a sphere of radius a moving through a viscous fluid (28, 29):

$$F_s = 6\pi\eta a U. \tag{B-1}$$

Here η is the viscosity of the fluid, and U is the velocity of the sphere relative to the velocity of infinitely distant fluid.

The velocity U in Eq. B-1 is replaced by the difference between hv_{zm}, the velocity of the myosin-drawn spheres, and $\overline{v_{zs}}$, the effective average velocity of the endoplasm in *Region I* as judged by the sphere. $\overline{v_{zs}}$ is estimated by averaging the Eq. A-10 velocity over the surface area of the sphere centered at $y = \epsilon/2$. The result is (39):

$$\overline{v_{zs}} = \frac{F_z}{2\eta_1} [\epsilon^2(\kappa - 1/4) - a^2/3]. \tag{B-2}$$

Taking the radius of the sphere as $a = \epsilon/2$ and using Eqs. A-15, B-1, and B-2, the force exerted on the endoplasm by a single sphere becomes

$$F_s = 3\pi\eta_1 \epsilon v_{zm} \left[h - \frac{(\kappa - 1/3)}{\kappa^2} \right]. \tag{B-3}$$

The spacing between adjacent actin bundles is s, and the center-to-center spacing between adjacent spheres on an actin bundle is q. The number of spheres per unit area of endoplasm-ectoplasm interface is then $s^{-1}q^{-1}$. If the interaction between these spheres is negligible, then the total force per unit area exerted by the spheres on the endoplasm is $F_s/(sq)$ or

$$F_{za} = \frac{3\pi\eta_1\epsilon v_{zm}}{sq}\left[h - \frac{(\kappa - 1/3)}{\kappa^2}\right]. \tag{B-4}$$

APPENDIX C: MOTIVE FORCE AND VELOCITY PROFILE GENERATED BY A MOVING ENDOPLASMIC NETWORK

An estimate is needed for the drag force between the fluid and the network of cylinders. The cubic lattice of the network is aligned with the coordinate axes so that the cylinders run parallel to the x-, y-, and z-axes. The cylinders all have radius a, and the center-to-center spacing between adjacent parallel cylinders is b, where $b \gg a$. A fluid of viscosity η flows through the network with superficial (average) velocity U in the z-direction.

For those cylinders parallel to the z-axis, the direction of fluid flow, the drag force per unit length of each cylinder is given by an equation of the same form as Eq. A-18:

$$F_n = \frac{2\pi\eta U}{\ln(b/a) - 1.32}. \tag{C-1}$$

For those cylinders parallel to the x- or y-axes, the average fluid velocity is perpendicular to the cylinder axes. For this orientation the drag force per unit length of cylinder is (29):

$$F_p = \frac{4\pi\eta U}{\ln(b/a) - 1.07}. \tag{C-2}$$

If the interaction between nonparallel cylinders is assumed negligible, then the drag force on the network can be estimated by summing Eqs. C-1 and C-2 over all cylinder lengths in a large volume of network. F_n, the drag force per unit volume of network, is then (39):

$$F_n = \frac{2\pi\eta fU}{b^2}, \tag{C-3}$$

where

$$f = \left[\frac{4}{\ln(b/a) - 1.07} + \frac{1}{\ln(b/a) - 1.32}\right]. \tag{C-4}$$

Eq. C-3 is applied to the model of streaming posed in Fig. 3 a. The motive force per unit volume applied to the fluid in Regions I and III is $F = 0$. In Region II the motive force is directed along the z-axis and has magnitude given by Eq. C-3, with the velocity U replaced by the difference between the network velocity, v_n, and the velocity of the endoplasm, v_z:

$$F_n = \frac{2\pi\eta_2 f(v_n - v_z)}{b^2}. \tag{C-5}$$

The network is assumed to be sufficiently rigid that v_n is a constant throughout Region II. The endoplasmic velocity, v_z, will not be a constant in Region II but will vary with position y. Eq. C-5 can be treated as a continuous function of y provided that changes in v_z are small over distances comparable to the network spacing b.

The equations of motion for the superficial endoplasmic velocity are again Eqs. A-2 and A-3. As in the calculation for Model A, the planar geometry of Fig. 3 a further simplifies these equations. Using Eq. C-5 for the motive force per unit volume in Region II, the equations of motion become:

in Regions I and III,

$$\frac{d^2 v_z}{dy^2} = 0; \tag{C-6}$$

in Region II,

$$\frac{d^2 v_z}{dy^2} + \frac{2\pi f(v_n - v_z)}{b^2} = 0. \tag{C-7}$$

The boundary conditions on v_z are again given by Eqs. A-6–A-9.

Eqs. C-6 and C-7 can be solved by standard techniques (38). Application of the boundary conditions then gives the complete solution for v_z:

in Region I ($0 \leq y \leq \epsilon$),

$$v_z = \frac{v_n y}{\epsilon}\left\{\frac{\sinh[k(\delta - \epsilon)] + \beta\cosh[k(\delta - \epsilon)] - \beta}{(\alpha + \beta)\cosh[k(\delta - \epsilon)] + (1 + \alpha\beta)\sinh[k(\delta - \epsilon)]}\right\}; \tag{C-8}$$

in Region II ($\epsilon \leq y \leq \delta$),

$$v_z = v_n\left\{1 - \frac{\alpha\cosh[k(\delta - y)] + \alpha\beta\sinh[k(\delta - y)] + \beta\cosh[k(y - \epsilon)] + \alpha\beta\sinh[k(y - \epsilon)]}{(\alpha + \beta)\cosh[k(\delta - \epsilon)] + (1 + \alpha\beta)\sinh[k(\delta - \epsilon)]}\right\}; \tag{C-9}$$

in Region III ($\delta \leq y \leq \gamma$),

$$v_z = v_n\frac{(\gamma - y)}{(\gamma - \delta)}\left\{\frac{\sinh[k(\delta - \epsilon)] + \alpha\cosh[k(\delta - \epsilon)] - \alpha}{(\alpha + \beta)\cosh[k(\delta - \epsilon)] + (1 + \alpha\beta)\sinh[k(\delta - \epsilon)]}\right\}; \tag{C-10}$$

where

$$k = \frac{\sqrt{2\pi f}}{b}, \tag{C-11}$$

$$\alpha = \frac{\eta_1}{\eta_2 k\epsilon}, \tag{C-12}$$

and

$$\beta = \frac{\eta_3}{\eta_2 k(\gamma - \delta)}. \tag{C-13}$$

The maximum velocity in the cell occurs in Region II at the position y given by the solution to the following transcendental equation:

$$\alpha\sinh[k(\delta - y)] + \alpha\beta\cosh[k(\delta - y)]$$
$$- \beta\sinh[k(y - \epsilon)] - \alpha\beta\cosh[k(y - \epsilon)] = 0. \tag{C-14}$$

The motive force F_{za} applied per unit area of the endoplasm-ectoplasm interface is calculated by substituting Eq. C-9 into Eq. C-5 and integrating the resulting expression for F_n over the interval $\epsilon \leq y \leq \delta$. The result is

$$F_{za} = v_n\eta_2 k\left\{\frac{(\alpha + \beta)\sinh[k(\delta - \epsilon)] + 2\alpha\beta\cosh[k(\delta - \epsilon)] - 2\alpha\beta}{(\alpha + \beta)\cosh[k(\delta - \epsilon)] + (1 + \alpha\beta)\sinh[k(\delta - \epsilon)]}\right\}. \tag{C-15}$$

The drag F_{zw} on the endoplasm-ectoplasm interface wall is calculated from the velocity gradient at the wall and is given by

$$F_{zw} = \frac{v_n\eta_1}{\epsilon}\left\{\frac{\sinh[k(\delta - \epsilon)] + \beta\cosh[k(\delta - \epsilon)] - \beta}{(\alpha + \beta)\cosh[k(\delta - \epsilon)] + (1 + \alpha\beta)\sinh[k(\delta - \epsilon)]}\right\}. \tag{C-16}$$

APPENDIX D: LIMITATIONS ON THE HYDRODYNAMICS PRESENTED FOR THE THREE MODELS

The simple hydrodynamic analyses presented here are subject to several limitations that should be recognized. All models are simplified by use of planar geometry rather than the actual cylindrical geometry of the algal cell. Since the thickness of the endoplasm ($10 \mu m$) is much less than the radius of curvature of the endoplasm-ectoplasm interface ($350 \mu m$), the planar geometry calculations give a good approximation for flow in the endoplasm. Although flow in the vacuole cannot be precisely modeled with planar geometry, the comparatively large radius of the vacuole guarantees a slow velocity gradient in the vacuole and a negligible effect on streaming in the endoplasm.

The drag formulas for cylinders (Eqs. A-18, C-1, and C-2) and spheres (Eq. B-1) as used here take into account neither the effect of nearby walls nor, in the case of Eqs. B-1 and B-4, the effect of particle interactions. Neglect of the wall effect underestimates the motive force (Eqs. A-21 and B-4), since the drag per particle increases for particles moving parallel to a nearby wall (29, 40). On the other hand, neglect of particle interactions overestimates the motive force, since the drag per particle decreases for particles moving as a group (29). Being of comparable magnitude (29), these effects offset each other to reduce the overall error.

Another limitation of Models A and B arises from use of the velocity profile (Eq. A-10) obtained from the somewhat arbitrary assumption (7) of constant motive force per unit volume in Region I (Eq. A-4). The error introduced here should not be large, however, because the requirement of a very steep velocity gradient at the wall (Empirical Characteristics: Velocity Profile) guarantees that the real velocity profile cannot be very different from Eq. A-10.

In Model C the *Region II* velocity profile (Eq. C-9) is probably not exactly correct for *y* near ε. In solving Eq. C-7 for the velocity profile, the motive force (Eq. C-5) was treated as a continuous function of *y*. This approach assumes that the velocity v_z in *Region II* changes only slowly over distances comparable to the lattice spacing *b*. Sizeable velocity gradients at *y* near ε in *Region II* do occur with those Table III parameter sets for which $y_{0.9} > \epsilon$. Although Eq. C-9 is less accurate for these parameter sets, it remains clear that the velocity increases very rapidly away from the wall and reaches essentially the network velocity within one or two lattice units into the network.

Other inaccuracies may arise from non-Newtonian properties of the endoplasm. Newtonian results for Models A and B (Tables I and II) show that myosin or myosin-sphere velocity along the actin bundles must often be more than twice the endoplasmic velocity, i.e., $h > 2$. When $h > 2$ is required, the shear rate at the actin bundles has opposite algebraic sign and greater magnitude than the shear rate at the endoplasm-ectoplasm interface wall. Since the apparent viscosity of non-Newtonian endoplasm decreases at greater shear rate (23, 24), the balance between viscous forces exerted by the motile elements (myosin or myosin-spheres) and the wall may require an even greater speed factor *h* to compensate for lower viscosity at the actin bundles. This consideration may partially explain the difference between the $h = 6.5$ calculated by Hayashi (12) for a non-Newtonian model and the $h = 3.57$ calculated here (Table I, parameter set 7A) for a somewhat similar but Newtonian model.

REFERENCES

1. Korn, E. D. 1978. Biochemistry of actomyosin-dependent cell motility. *Proc. Natl. Acad. Sci. U. S. A.* 75:588–599.
2. Allen, N. S., and R. D. Allen. 1978. Cytoplasmic streaming in green plants. *Annu. Rev. Biophys. Bioeng.* 7:497–526.
3. Kamiya, N. 1981. Physical and chemical basis of cytoplasmic streaming. *Annu. Rev. Plant Physiol.* 32:205–236.
4. Nothnagel, E. A., L. S. Barak, J. W. Sanger, and W. W. Webb. 1981. Fluorescence studies on modes of cytochalasin B and phallotoxin action on cytoplasmic streaming in *Chara. J. Cell Biol.* 88:364–372.
5. Nothnagel, E. A., J. W. Sanger, and W. W. Webb. 1982. Effects of exogenous proteins on cytoplasmic streaming in perfused *Chara* cells. *J. Cell. Biol.* 93:735–742.
6. Allen, N. S. 1974. Endoplasmic filaments generate the motive force for rotational streaming in *Nitella. J. Cell Biol.* 63:270–287.
7. Donaldson, I. G. 1972. The estimation of the motive force for protoplasmic streaming in *Nitella. Protoplasma.* 74:329–344.
8. Donaldson, I. G. 1972. Cyclic longitudinal fibrillar motion as a basis for steady rotational protoplasmic streaming. *J. Theor. Biol.* 37:75–91.
9. Pickard, W. F. 1972. Further observations on cytoplasmic streaming in *Chara braunii. Can. J. Bot.* 50:703–711.
10. Pickard, W. F. 1974. Hydrodynamic aspects of protoplasmic streaming in *Chara braunii. Protoplasma.* 82:321–339.
11. Hayashi, Y. 1980. Fluid-dynamical study of protoplasmic streaming in a plant cell. *J. Theor. Biol.* 85:451–467.
12. Hayashi, Y. 1980. Theoretical study of motive force of protoplasmic streaming in a plant cell. *J. Theor. Biol.* 85:469–480.
13. Ewart, A. J. 1903. On the Physics and Physiology of Protoplasmic Streaming. Clarendon Press, London, England.
14. Kamiya, N., and K. Kuroda. 1956. Velocity distribution of the protoplasmic streaming in *Nitella* cells. *Bot. Mag. Tokyo.* 69:544–554.
15. Mustacich, R. V., and B. R. Ware. 1974. Observation of protoplasmic streaming by laser-light scattering. *Phys. Rev. Lett.* 33:617–620.
16. Mustacich, R. V., and B. R. Ware. 1976. A study of protoplasmic streaming in *Nitella* by laser Doppler spectroscopy. *Biophys. J.* 16:373–388.
17. Langley, K. H., R. W. Piddington, D. Ross, and D. B. Sattelle. 1976. Photon correlation analysis of cytoplasmic streaming. *Biochim. Biophys. Acta.* 444:893–898.
18. Sattelle, D. B., and P. B. Buchan. 1976. Cytoplasmic streaming in *Chara corallina* studied by laser light scattering. *J. Cell Sci.* 22:633–643.
19. Mustacich, R. V., and B. R. Ware. 1977. Velocity distributions of the streaming protoplasm in *Nitella flexilis. Biophys. J.* 17:229–241.
20. Sattelle, D. B., D. J. Green, and K. H. Langley. 1979. Subcellular motions in *Nitella flexilis* studied by photon correlation spectroscopy. *Physica Scripta.* 19:471–475.
21. Kamiya, N., and K. Kuroda. 1958. Measurement of the motive force of the protoplasmic rotation in *Nitella. Protoplasma.* 50:144–148.
22. Tazawa, M. 1968. Motive force of the cytoplasmic streaming in *Nitella. Protoplasma.* 65:207–222.
23. Kamiya, N., and K. Kuroda. 1973. Dynamics of cytoplasmic streaming in a plant cell. *Biorheology.* 10:179–187.
24. Kamiya, N., and K. Kuroda. 1965. Rotational protoplasmic streaming in *Nitella* and some physical properties of the endoplasm. *In* Proceedings of the Fourth International Congress on Rheology. A. L. Copley, editor. John Wiley & Sons Inc., New York. Part 4:157–171.
25. Allen, R. D. 1977. Concluding remarks. *In* International Cell Biology. B. R. Brinkley and K. R. Porter, editors. Rockefeller University Press, New York. 403–406.
26. Bradley, M. O. 1973. Microfilaments and cytoplasmic streaming: inhibition of streaming with cytochalasin. *J. Cell Sci.* 12:327–343.
27. Nagai, R., and L. I. Rebhun. 1966. Cytoplasmic microfilaments in streaming *Nitella* cells. *J. Ultrastruct. Res.* 14:571–589.
28. Landau, L. D., and E. M. Lifshitz. 1959. Fluid Mechanics. Pergamon Press Ltd., London, England.
29. Happel, J., and H. Brenner. 1965. Low Reynolds Number Hydrodynamics. Prentice-Hall, Inc., Englewood Cliffs, NJ.
30. Purcell, E. M. 1977. Life at low Reynolds number. *Am. J. Phys.* 45:3–11.
31. Williamson, R. E. 1975. Cytoplasmic streaming in *Chara*: a cell model activated by ATP and inhibited by cytochalasin B. *J. Cell Sci.* 17:655–668.
32. Nagai, R., and T. Hayama. 1979. Ultrastructure of the endoplasmic factor responsible for cytoplasmic streaming in *Chara* internodal cells. *J. Cell Sci.* 36:121–136.
33. Williamson, R. E. 1979. Filaments associated with the endoplasmic reticulum in the streaming cytoplasm of *Chara corallina. Eur. J. Cell Biol.* 20:177–183.
34. Allen, N. S. 1980. Cytoplasmic streaming and transport in the characean alga *Nitella. Can. J. Bot.* 58:786–796.
35. Durham, A. C. H. 1974. A unified theory of the control of actin and myosin in nonmuscle movements. *Cell.* 2:123–136.
36. Yano, M. 1978. Observation of steady streamings in a solution of Mg-ATP and acto-heavy meromyosin from rabbit skeletal muscle. *J. Biochem. (Tokyo).* 83:1203–1204.
37. Yano, M., T. Yamada, and H. Shimizu. 1978. Studies of the chemo-mechanical conversion in artificially produced streamings. I. Reconstruction of a chemo-mechanical system from acto-HMM of rabbit skeletal muscle. *J. Biochem. (Tokyo).* 84:277–283.
38. Ross, S. L. 1964. Differential Equations. Ginn and Co., Boston, MA.
39. Nothnagel, E. A. 1981. Studies on the mechanism of cytoplasmic streaming in *Chara corallina.* Doctoral Thesis. Cornell University, Ithaca, NY.
40. O'Neill, M. E., and K. Stewartson. 1967. On the slow motion of a sphere parallel to a nearby plane wall. *J. Fluid Mech.* 27:705–724.